

ROSETTA COMMAND AND MONITORING OPERATIONS FOR PHILAE LANDING

**Federico Zuiani^(1,2), Francesco Castellini^(1,3), Sabine Kielbassa^(1,4), Carlos Bielsa^(1,5) and
Juan Manuel Garcia^(1,6)**

⁽¹⁾ ESOC, Robert-Bosch-Straße 5, 64293 Darmstadt Germany

⁽²⁾ CGI Deutschland Ltd. & Co., federico.zuiani@cgi.com

⁽³⁾ Telespazio VEGA Deutschland GmbH, Francesco.Castellini@esa.int

⁽⁴⁾ Telespazio VEGA Deutschland GmbH, Sabine.Kielbassa@esa.int

⁽⁵⁾ GMV, cbielsa@gmv.com

⁽⁶⁾ GMV, jgarcia@gmv.com

Abstract: *The paper focuses on the contributions of Flight Dynamics monitoring and commanding activities for the delivery of Philae from Rosetta to the surface of comet 67P on the 12th of November 2014. A set of quantitative assessments from spacecraft telemetry and dynamic analyses performed in the preceding months and weeks is presented, which allowed verifying the suitability of the space and ground segments to satisfy the tight performance requirements for the delivery. The design of Rosetta's operational timeline and attitude profile for the landing phase is also described, and the main results from actual operations are presented, showing how all preparation activities contributed to achieving the first soft landing on the surface of a comet.*

Keywords: *Comet landing, command generation, AOCMS monitoring.*

1. Introduction

On November 12th 2014, the European Space Agency's Philae Lander was released by the Rosetta spacecraft and, 7 hours later, achieved the first-ever soft landing on a cometary nucleus. Such an accomplishment required a large effort from the Flight Dynamics (FD) team at ESOC, and this paper describes in detail the FD activities carried out in preparation for the landing and during the critical operations that started about one day before separation. The focus of this paper is on the contribution of spacecraft commanding and monitoring activities to the success of the Philae landing. This includes detailed assessments of several aspects of the spacecraft (SC) health in the weeks before separation, a variety of analyses and simulation exercises involving the SC and its interaction with the environment, and the design and flawless execution of the operational timeline from pre-delivery trajectory to Lander relay phase.

Several other papers provide a broader overview of the Rosetta mission from reactivation to landing from a Flight Dynamics perspective. In particular, [1] summarizes the comet phase FD operations, whereas others focus on the critical optical measurements ([2], [3]) and on the orbit determination ([4], [5]) for the Rosetta SC. The navigation activities specifically targeted to the release of Philae in November are instead covered in [6], which describes both the trajectory of Rosetta before and after separation, and the descent and rebound dynamics of Philae. In this context, the present paper provides a detailed analysis of the FD commanding and SC monitoring activities, which contributed – together with the very accurate comet knowledge (gravity, shape, coma) gained in the characterization phase ([5]), sound landing trajectory design and precise navigation ([6]) – to achieving a first touch-down point merely 118 meters from Philae's target coordinates on the surface of 67P/Churyumov-Gerasimenko.

A variety of dynamics analyses, spacecraft health assessments and simulation exercises will be presented in the paper. These were conducted in the course of the brief comet characterization phase, both to verify the feasibility of the planned separation and landing operations and to inform the design of the detailed timeline of activities.

The monitoring of the SC health included analyses of the telemetry (TM) of star trackers and coarse sun sensors in the weeks before separation, to assess the likelihood of interference of coma dust particles on the SC sensors. Moreover, particular care was taken of the Reaction Wheels status, with continuous assessments of the friction torques and imposition of limitations on both maximum speeds and zero-crossings, to ensure the availability of all four wheels during the slews before and after separation. Finally, an analysis of the stability of the accelerometer bias over the manoeuvres during approach and comet phase, led to the decision of allocating a long calibration slot with the SC in Δv attitude just before the Orbiter pre-delivery manoeuvre. This in fact would allow for precise accelerometer bias calibration in an environment of thermal stability, critical to ensure the required Δv accuracy, largely affecting the landing coordinates.

Additional preparation activities informing the design of respectively the pre-delivery orbits and the landing timeline regarded the simulation of navigation images and the modelling of the Lander separation dynamics. In particular, the comet illumination and landmarks visibility over the critical hours leading to the data cut-off for the final orbit determination and optimization of the landing sequence was verified with realistic simulations of the scheduled optical images, concluding that there would be sufficient information to reconstruct the SC state within required accuracy. The effects of Lander ejection on the spacecraft attitude and angular momentum, both during the ejection process and the subsequent transient, were instead analytically assessed, and results led to the decision of not to pre-compensate the spacecraft attitude.

The design and successive flawless execution of the operational timeline, covering pre-delivery trajectory, separation and Lander relay phases, was the last main contribution of the commanding and TM monitoring subsystems to the success of the Philae landing. A remarkable number of complex activities was accommodated in a few hours around Lander separation (i.e. from -12 hours to +12 hours), including three Δv manoeuvres (also known as Orbit Control Manoeuvres or OCMs), several Wheel Off-Loadings (WOLs), complex attitude rasters for optical imaging of the comet nucleus and the descending Lander, high gain antenna steering and a variety of AOCS mode changes. Furthermore, several GO/NOGO decision points were envisaged involving close interaction among the different subsystems, including one based on Δv performance soon after the reception of Doppler data for the pre-delivery OCM. The sequence of events during the delivery phase will be presented, in particular from the attitude and AOCMS modes, guidance, and commands point of view.

In the following sections, all details of the aforementioned topics are presented, focusing first on the spacecraft monitoring and dynamic analysis activities in preparation of the landing, and then on the design of the attitude profile and mission timeline. Finally, telemetry results from actual operations are provided, confirming their contribution to the success of the landing.

2. Spacecraft monitoring and image simulations in preparation of Philae landing

This section outlines the assessments of SC telemetry and the simulation of comet imagery performed in preparation of the landing. First, data from TM are presented, highlighting the most critical aspects for comet proximity operations, in particular the robustness of the attitude sensors to the dust environment, the behaviour of the reaction wheels and the stability of the acceleration measurements. Then, a few examples are given of the simulation of images to be taken during

the pre-delivery orbit, extremely critical for ensuring an accurate navigation in the final leg before Philae's separation.

2.1 Rosetta spacecraft from a Flight Dynamics perspective

The Rosetta SC is constituted of a 3-axis stabilized platform with an Attitude and Orbit Control and Measurement System (AOCMS) which is relatively standard for interplanetary missions. It makes use of 2 Star Trackers (STR), 4 Coarse Sun Sensors (CSS) and 2 Inertial Measurement Packages (IMP) for attitude estimation and manoeuvres cut-off, and of 4 Reaction Wheels (RW) and 24 Reaction Control Thrusters (RCT) for both attitude and orbit control. Moreover, Rosetta is equipped with two Navigation Cameras (Navcams) for optical navigation, as described in [2] and [3]. Figure 1 shows the configuration of the spacecraft, with the main units used for AOCMS circled in red. Also several payloads are used by FD for operational reasons, in particular the Osiris science cameras for complementing the Navcams and the Rosina pressure sensor for coma modelling. Rosetta's large Solar Arrays (SA), not shown in the picture, protrude from +/-Y faces, and can rotate around +/-Y to maximise the amount of incident radiation, whereas the High Gain Antenna (HGA) can rotate in both elevation (Y) and azimuth (Z). The 4 RCT normally used for OCMs (plus 4 redundant ones) are located on the -Z face and provide a force along +Z. Finally, the Lander was located on the -X face, with the ejection direction almost perfectly aligned with -X (2.4 deg offset).

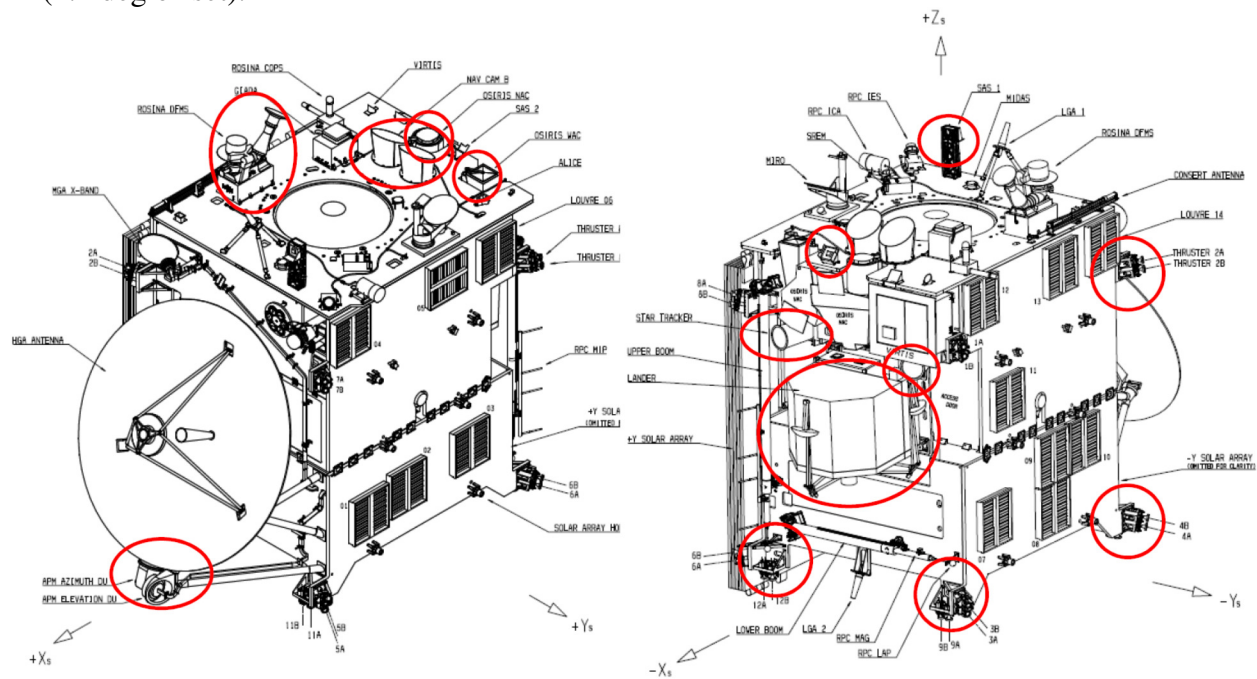


Figure 1: Rosetta spacecraft from a Flight Dynamics perspective

2.2 Attitude sensors monitoring

Rosetta uses 2 STRs in cold redundancy for attitude determination in nominal mode, and CSS for safe mode recovery. Both types of sensor can encounter serious issues in an active comet environment, when the SC is flying inside a cloud of dust and gases. Although this was already known at the conceptual stage of the mission and some special features were therefore

incorporated in the design (e.g. special STR algorithms to partially cope with dust particles), specific monitoring measures have been taken by FD to ensure the safety of the SC.

Regarding the sun sensors, a very dangerous situation would arise if reflected sunlight from both the comet nucleus and its coma was to induce currents higher than the on-board Sun detection threshold. If that is exceeded, in case of a safe mode the SC may lock to the comet direction rather than the Sun's, possibly resulting in loss of mission. Therefore, starting from the arrival at comet 67P in August 2014, the total current detected on the -XZ CSS (almost never facing the Sun) has been regularly monitored, with the purpose of raising a warning and increasing the detection threshold in time, if necessary. In the months leading to the landing, nothing more than current noise has however been observed, suggesting that sun acquisition would have occurred, as verified in a safe mode later in March 2015. In the continuation of the mission and throughout the comet's perihelion pass in August 2015, the current levels have never spiked above worrying levels, confirming that 67P's environment is not sufficiently bright to cause CSS issues.

Of a totally different scale has instead been the effect on Rosetta's operations of the STR's capability to track stars within the cometary environment. It was already known since the design phase, that because of this the SC would have not been able to successfully navigate very close to the nucleus at Sun distances well below 3 AUs, which is the reason why Philae's landing date was set to the beginning of November 2014, even though this only allowed for a very short time frame for comet characterization and landing preparations. In order to verify the SC's suitability for close proximity operations, the STR behaviour has been closely monitored by the FD team, and continues to be routinely checked now.

Four main indicators are used: the number of tracked stars (maximum 9), the noise on the SC off-pointing especially on the X axis (STR boresight), the maximum innovation from the stellar estimator (i.e. maximum angular difference between tracked and predicted position of the stars in the Field of View FoV) and the STR background level. Before landing, these provided the necessary evidence that, as expected, Rosetta was capable of approaching the nucleus as required for Philae's separation, mapping the comet's shape, gravity and gas environment down to less than 10 km from the surface. In fact, the STR was continuing to track enough stars (always above 7, whereas 2 is the minimum for attitude reconstruction) with very smooth off-pointing profile (noise in stable pointing ~1 mdeg, similar to deep space), maximum innovation below 1 STR pixel (15 mdeg) and background levels ~90 mV/s similar to deep space. Figure 2 and Figure 3 show the trends of these parameters in October 2014, before the landing, in comparison with September 2015, close to maximum comet activity. Even though the 2015 data are referred to distances of more than 300 km from the comet vs. 10-30 km of the landing period, all indicators show much worse behaviour, with spikes to 2/3 pixels of innovation, 10 mdeg off-pointing, ~110 V/s background and several occasions with STR loss of tracking. The worse conditions have actually been encountered in the period March to July 2015, when Rosetta was kept as close as possible to the nucleus for better science and Lander communications. In this period, besides regularly losing and reacquiring tracking, in several instances the STR in the loop triggered a FDIR on the consistency of gyro and STR measurements, leading to reconfigurations to the redundant side. In two occasions, none of the star trackers was able to acquire for up to 1 day, resulting in an off-pointing due to the cumulated gyro bias error of up to ~0.6 deg, when the initial symptoms of HGA loss of pointing were felt. Twice more, STR issues led to safe modes, recovered due to successful star acquisitions without switching to the so-called – and particularly critical – “survival” safe mode. In fact, the whole trajectory of Rosetta starting from the first months of 2015 has been the result of the compromise between the desire of staying as close as

possible to 67P for both science and Lander communications, and the necessity of staying far enough for sufficient STR performance and hence safe operations.

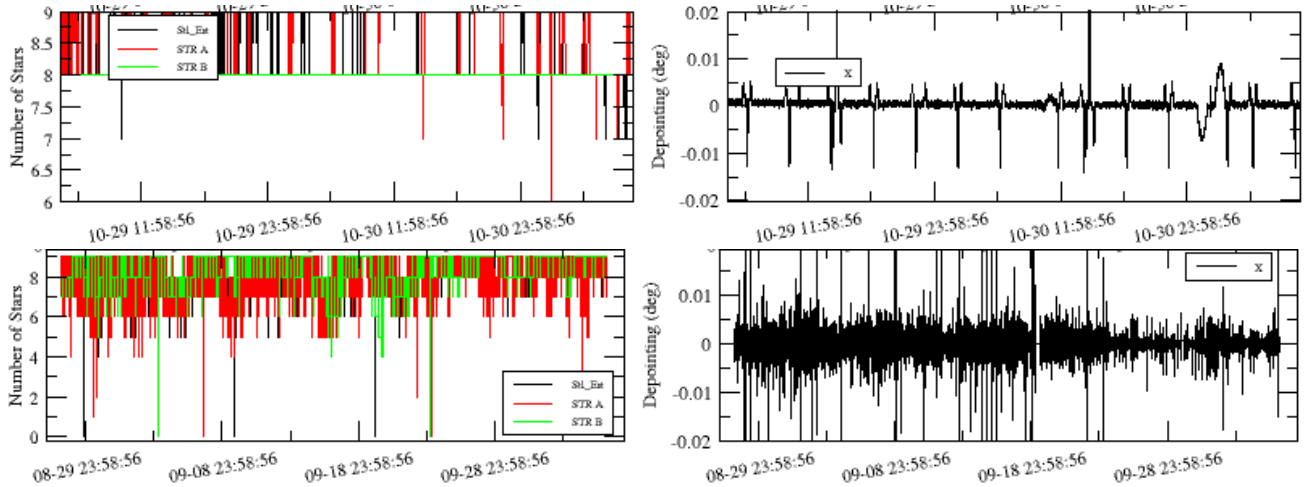


Figure 2: Number of tracked stars and SC de-pointing noise on X axis for October 2014 (top) and September 2015 (bottom).

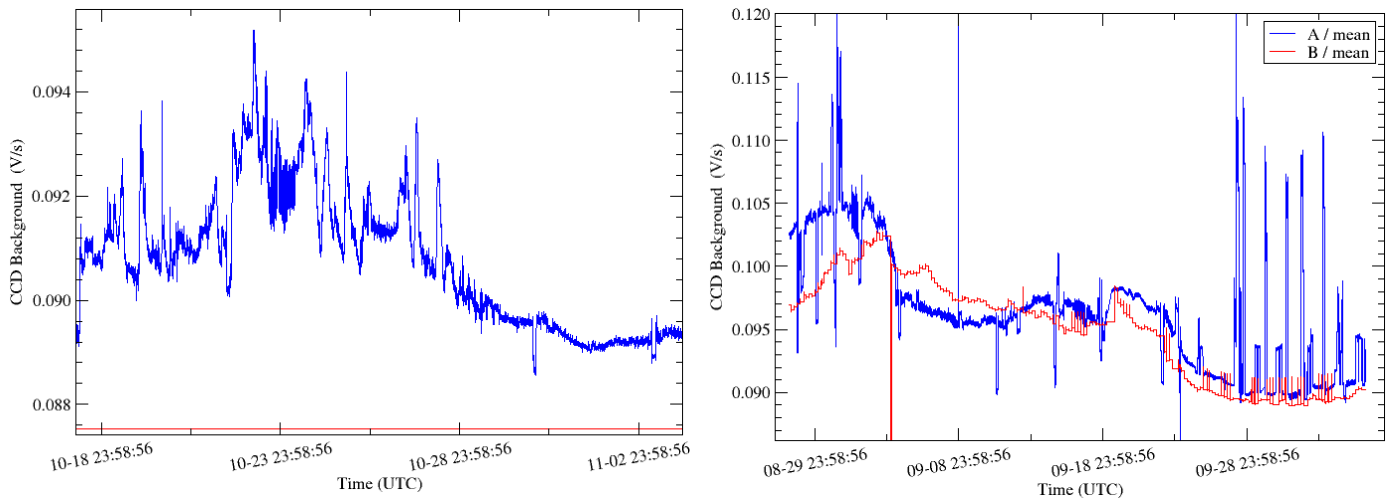


Figure 3: STR background level in October 2014 and September 2015

Two additional methods for STR health monitoring have also been devised. On one side, the redundant STR has been regularly switched on, several times daily, to verify its capability to acquire from “lost-in-space” conditions, which is by far more difficult than keeping tracking. Throughout 2015, as soon as such acquisition attempts were starting to be partially unsuccessful, the distance of the SC from the nucleus was increased, ensuring that, in case of inconsistencies triggering a STR reconfiguration or even a safe mode, the SC would have been able to safely return to HGA Earth pointing. On the other hand, images of the empty sky have been taken in several occasions with both Navcam and STR, to characterize the dust environment. Figure 4 shows examples of such images from July 2015. Large numbers of particles are evident from the images, even showing defocused objects very close to the SC. According to the manufacturer, Rosetta’s STR is capable of successfully acquiring an attitude with at most 1000 false stars in the FoV. In the STR CCD dump tests, no significant degradation of the performance was initially detected, with at most 150 “false stars”. This started to change in May 2015, when a CCD dump

revealed 436 non stellar objects with a magnitude lower than 5.4 (the limit of the on-board star catalogue), proving how marginal the operability of the SC at the current comet distances was. As a consequence of all these assessments, it was finally decided around the beginning of August to retreat at safer distances, where Rosetta will remain until December 2015, when the increasing Sun distance will again allow closer investigations. In spite of all the encountered issues, the STR monitoring efforts have allowed to both verify the safe conduction of comet landing operations in November 2014, and to safely carry the SC through perihelion in 2015.

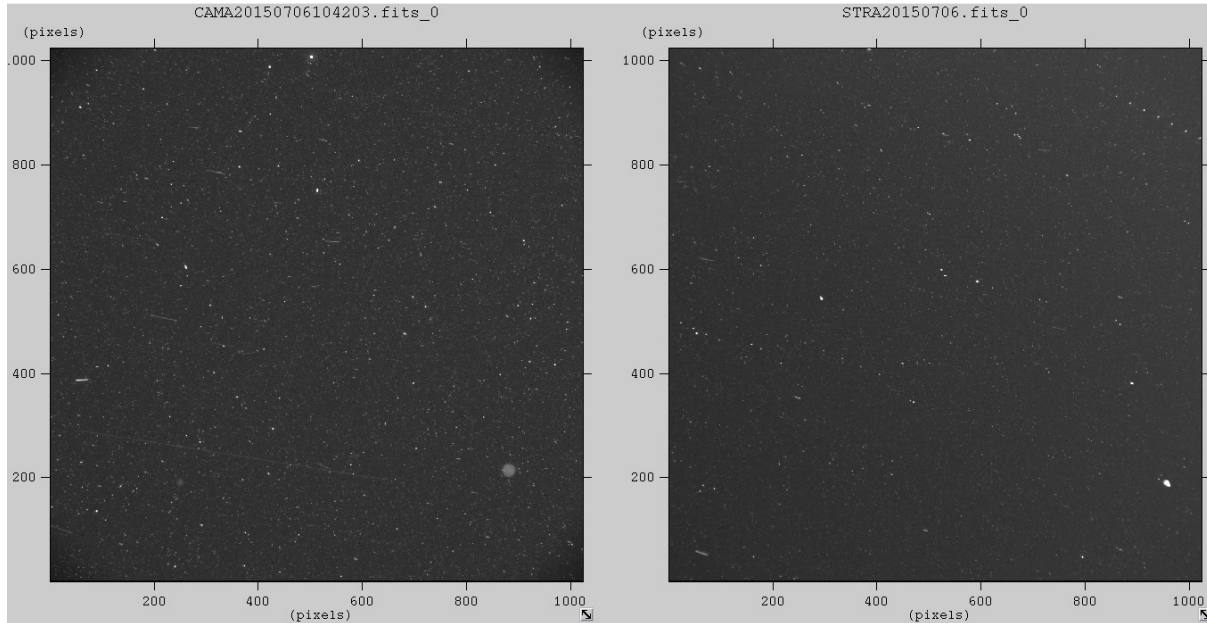


Figure 4: Navcam image of the empty sky and STR CCD dump from July 2015.

2.3 Reaction Wheels monitoring and speed optimization

Another critical equipment for Rosetta's operations is constituted by its RWs, which according to design specifications can reach up to 37.8 Nms of angular momentum load remaining within safe friction levels, defined by the manufacturer as 50 mNm. However, due to the long timespan of the mission and the fragile mechanical nature of the spinning wheels, already before hibernation RWs B and C were showing the first symptoms of degradation, i.e. cage instability at low speeds and higher than normal frictions at high speeds. For this reason, while on one side industrial activities led to the development of a two-wheel AOCMS mode already tested on the SC's Engineering Qualification Model on ground and ready to be patched on-board if necessary, mitigation actions have been taken within FD to reduce the likelihood of failures. These consisted in continuous monitoring of RWs health and optimization of the wheel off-loadings to minimize both the zero-crossings and high speed operations.

Figure 5 present the correlation between RW measured angular momentum and estimated friction torque in two different one-month time spans, before Lander delivery and in September 2015, clearly showing how wheel C now has the most critical behaviour. Particular attention was paid to the optimization of the central levels of the wheels after each wheel off-loading, as a function of the foreseen future slews, in order to minimize the stress on wheel C. This has paid off, as all RWs performed well during the critical Lander delivery phase when fast slews where required, and are still performing within the allowed limits almost one year later. RW C recently

showed a much worsened behaviour, with frictions reaching 40 mNm in a few zero-crossings (threshold for the reconfiguration to 3 wheels is set to 50 mNm) and unstable torques at the maximum speeds where it's now operated, but no FDIR has yet been triggered and both spacecraft and ground are ready for operations with 3 or even 2 wheels, if ever necessary.

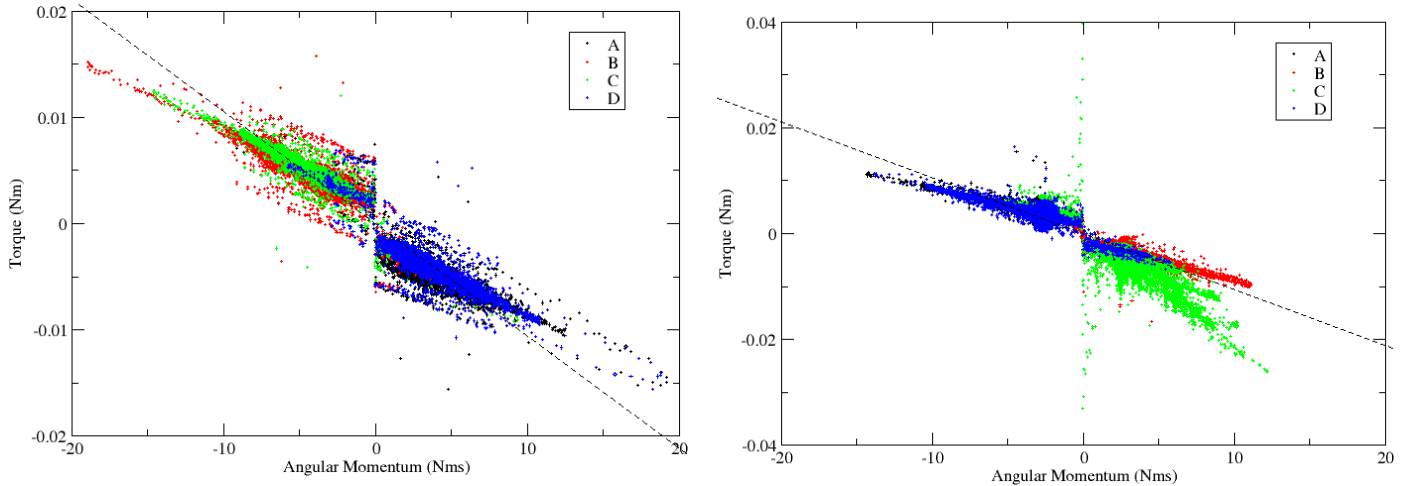


Figure 5: RW torque friction vs. speed in October 2014 (left) and September 2015 (right).

2.4 Accelerometers bias estimation

As described in more details in [6], a key driver for the final landing accuracy was the performance of the pre-delivery OCM, bringing Rosetta from the pre-delivery circular orbit at 30 km to the final descent trajectory for the release of Philae. And the key for an accurate OCM is a precise calibration of the accelerometers, from whose measurements the OCM is autonomously cut on-board. All accelerometers present a bias which is highly dependent on the temperature of the unit, typically large enough to create errors up to several percent of the manoeuvre size. As the maximum error considered in the landing navigation analysis for the pre-delivery OCM was of 0.5% on the Δv , the accelerometer measurements precision had to be carefully evaluated.

The bias calibration process consists in the simple differentiation of the cumulated linear velocity, which is the raw measurement of the IMPs, over a period of at least half an hour in order to minimize the effect of the read-out noise. This had been typically performed in the previous phases of the mission in stable attitudes about one day before the OCMs. However, from an analysis of the OCM performances in the months leading to the landing, it became clear that the change in bias due to the changing thermal environment would not allow to satisfy the requirement for the pre-delivery OCM. Figure 6 shows the oscillations of the estimated accelerometer bias for the 3 IMPs from May to November 2014, projected on the spacecraft's Z axis (i.e. the thrust direction). These were converted in the effect on a manoeuvre of the duration and size of the pre-delivery OCM, and the percentage difference of such effect with respect to the average bias is presented in Figure 7. The analysis led to two conclusions: first, all OCMs would be executed using IMP-A, which was identified as the one with the lowest contribution of the bias variations on the SC Z axis. Secondly, a calibration slot of 12 hours in the manoeuvre attitude would have to be included in the Lander delivery timeline (see Section 4), with all instruments and equipment in a stable power configuration. Only such an approach, allowing for thermal tranquilization of the SC and hence precise calibrations to be performed in the final few hours, would have ensured achieving the required OCM performance, as described in Section 5.

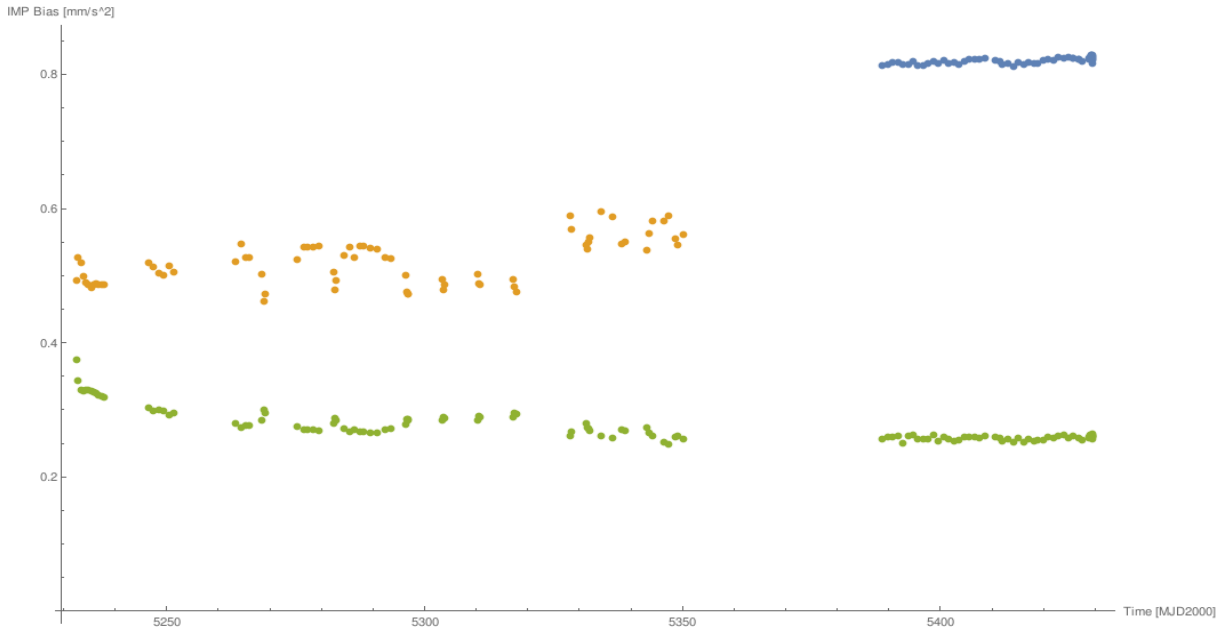


Figure 6: Accelerometer bias estimates in May-October 2014 projected on the SC Z axis.

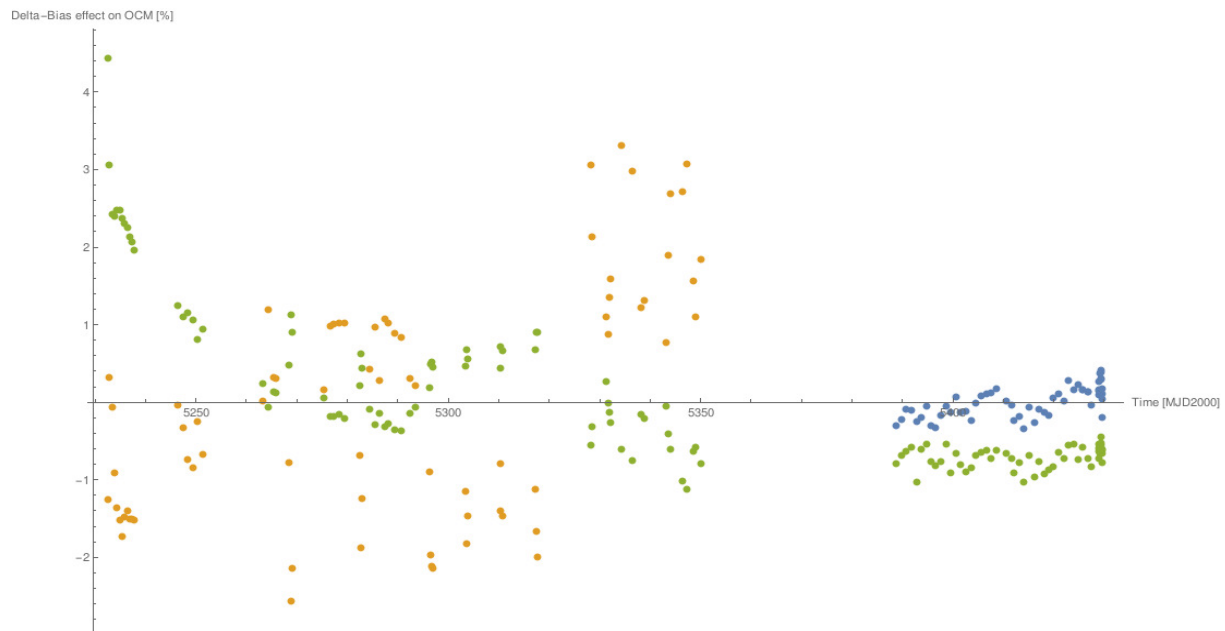


Figure 7: Effect of the bias on pre-delivery OCM, in percentage difference with respect to the average bias, from the May-October 2014 data, i.e. $(bzsc(j) - avg(bzsc)) \cdot t_{ocm} / \Delta V_{ocm} \cdot 100$.

2.5 Pre-delivery orbit images simulation

For organizational reasons, the AOCMS monitoring group of ESOC's FD team is also in charge of all optical measurements for Rosetta, and hence developed a wide range of software tools for the reduction of optical data into measurements for the orbit determination process. A detailed description of the developed algorithms and operational activities is given in [2] and [3], respectively for the comet centre data during approach and for the landmark observations during the near-comet phase. As a complementary tool for operations preparation, an image simulator

was developed with the purpose of generating synthetic images of the comet for the future planned trajectories, in order to verify their suitability for landmark-based navigation. The algorithm for the simulator is based on a modified Lunar reflectance photometric model and on high definition shape and albedo models. The photometric model was developed and specifically calibrated on the approach and proximity images of 67P/Churyumov-Gerasimenko, as detailed in [2]. Shape and albedo models were instead built using a combination of shape carving methods for coarse modelling and local maplets stitching for higher resolution, as described in [7].

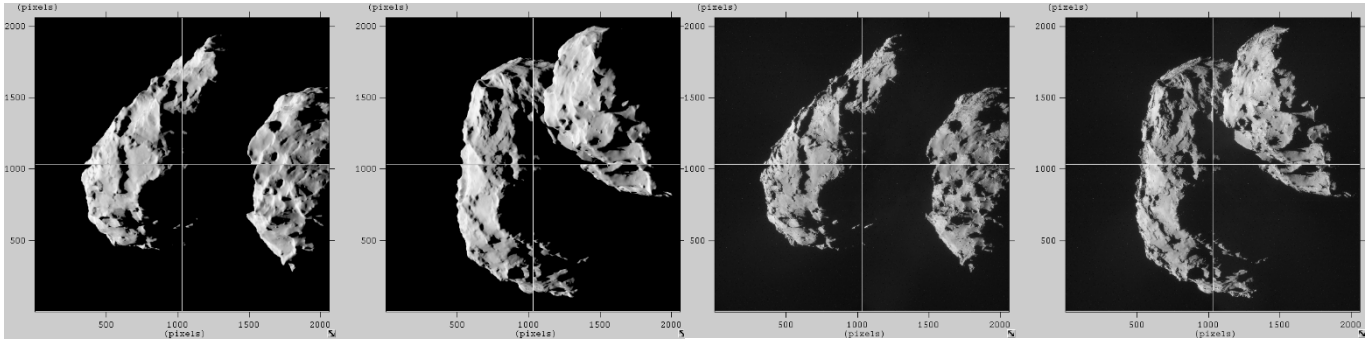


Figure 8: Rasters of 4 Navcam images from 10/11/2014. Left/right: simulated/actual images

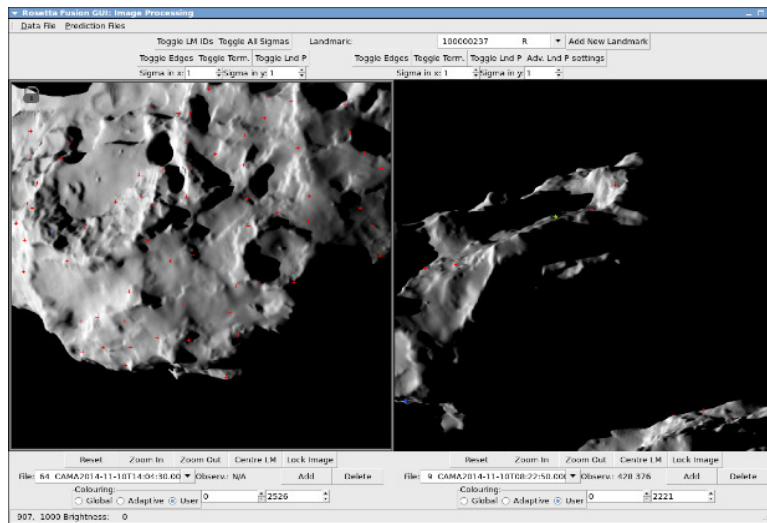


Figure 9: Simulated Navcam images from the pre-delivery orbit of the selected landing site, including landmark observations identified with the maplets method on the simulated data.

By using the best knowledge of the future spacecraft and target body orbits and attitudes from the orbit determination and propagation process, and the highest fidelity shape model available (4 million facets and 1 m resolution achieved with Navcam images in 10 km orbits of October 2014), it was possible to simulate 67P images very realistically. This is shown in Figure 8, where simulated and actual rasters of 4 navigation images are compared. Such capability is particularly useful for verifying if possible future trajectories will allow capturing enough illuminated comet parts for the identification of a sufficient number of landmarks. Even though body contour fitting and limb navigation methods were also developed (see [8]) and have been proven to effectively work for night side and far excursions throughout 2015, this verification was essential for the landing attempt. In fact, the availability of sufficient landmark observations in the period before the data cut-off for the latest orbit determination, upon which the final trajectory optimization for

the release of the Lander and the generation of all commands would have been based, was a FD Go/Nogo criterion. For this reason, during the landing site selection process, the trajectories prepared by FD for the different candidate sites proposed by the science teams were also tested for optical navigation suitability. Figure 8 reports examples of the simulated and actual rasters of 4 navigation images from about 20 hours before data cut-off, when Rosetta was on the 30 km predelivery orbit, clearly showing very large illuminated areas. Figure 9 then demonstrates the availability of landmark observations, when the maplets method was applied on the simulated data, finding between 9 and 64 landmarks in each of the images in the 30 hours of increased imaging frequency leading up to data cut-off. This was the final confirmation required to give a final approval to the Agilkia landing site and trajectory strategy, with the alternative candidates discarded for a variety of reasons, including for some a night side approach trajectory.

3. Lander ejection dynamics modelling

The Lander separation process comprised two phases:

- An initial phase of duration Δt_1 during which the Lander separated from the Orbiter with constant acceleration (1 m/s^2) until a given relative velocity Δv is reached.
- A second non-accelerated phase of duration Δt_2 until the Lander reached the end of the spindle (of total length 0.279 m).

The value of the target Δv could change between 0.05 m/s and 0.5 m/s. For the extreme values of Δv , the duration and relative distance covered by the Lander during the ejection process are listed in Table 1.

Table 1: Duration and relative distance covered by Lander during ejection

	$\Delta v = 0.05 \text{ m/s}$	$\Delta v = 0.5 \text{ m/s}$
Accelerated Phase	$\Delta t_1 = 0.05 \text{ s}$ $\Delta s_1 = 0.00125 \text{ m}$	$\Delta t_1 = 0.5 \text{ s}$ $\Delta s_1 = 0.125 \text{ m}$
Non-accelerated Phase	$\Delta t_2 = 5.555 \text{ s}$ $\Delta s_2 = 0.27775 \text{ m}$	$\Delta t_2 = 0.308 \text{ s}$ $\Delta s_2 = 0.154 \text{ m}$
Overall	$\Delta t = 5.605 \text{ s}$	$\Delta t = 0.808 \text{ s}$

In terms of mass properties, the ejection process had an effective lever arm of $\sim 0.075 \text{ m}$, creating mainly a torque around the SC's Y axis. The combined inertia of the system around the aforementioned axis was $\sim 1986 \text{ kg m}^2$. During the ejection process, both RWs of the SC and the Lander fly-wheel were storing some non-negligible angular momentum. The Lander fly-wheel was spun up to 5.2 Nms prior to the ejection. On the other hand, the maximum angular momentum on each of the SC Reaction Wheels was restricted to 37.8 Nms.

Because the attitudes of Lander and Orbiter were tied to one another, the spacecraft (SC) commanded attitude quaternion at separation was a key parameter to ensure a successful landing on the comet nucleus. Therefore, in preparation for the separation, a thorough analysis of the ejection dynamics was performed, including collection of data for the relevant parameters, development of the dynamic equations of separation, analysis of the orders of magnitude of the variables involved in the rotational movement of the Orbiter-Lander system during separation, and comparison against those derived from numerical solution of the equations and from the output of the SC simulator implanted by ESOC Flight Dynamics. Typical values for the angular offset and rate at separation were computed, and a sensitivity analysis was performed. The

impact on reaction wheel angular momentum was also assessed. The study was extended to include the dynamics of the Orbiter after separation. This section summarises the whole activity and provides the main results that were obtained.

3.1 Dynamics Equations during Ejection ignoring Flexible Modes

From Newton's law of rotational motion applied to the system Orbiter-Lander, and taking into account the characteristics of the ejection mechanism and of the Orbiter's PID attitude controller, the following system of differential equations is derived.

$$I_{comb}(t) \frac{d\vec{\omega}}{dt} + m_{comb} \dot{s}(t) \vec{r}_i \times \vec{e} + \vec{T}_{RW} + \vec{\omega} \times \vec{L}(t) + \frac{dI_{comb}(t)}{dt} \vec{\omega} = \vec{T}_{env}$$

Equation 1

$$\vec{T}_{RW} = H_{RW} \frac{d\hat{h}_{RW}}{dt}$$

Equation 2

$$\frac{dh_{RW,k}}{dt} = t_{RW,k} = \min\{t_k^{PID} \quad t_{RW,max}\} \text{sign}(t_k^{PID}) \quad k = 1, \dots, 4$$

Equation 3

$$\hat{t}^{PID} = \{t_1^{PID} \quad t_2^{PID} \quad t_3^{PID} \quad t_4^{PID}\} = H_{RW} \left(\vec{k}_p * \vec{\theta} + \vec{k}_d * \vec{\omega} + \vec{k}_i * \int \vec{\theta} dt \right)$$

Equation 4

$$\vec{\omega} = \frac{d\vec{\theta}}{dt}$$

Equation 5

with independent variables $\vec{\theta}(t)$, $\vec{\omega}(t)$ and $\hat{h}_{RW}(t)$, and initial conditions $\vec{\theta}(t=0) = \vec{0}$, $\vec{\omega}(t=0) = \vec{0}$ and $\hat{h}_{RW}(t=0) = \hat{h}_{RW}$. In the equation above, * denotes the component-by-component product, $\vec{\theta}(t)$ is the rotation of the system Orbiter-Lander relative to the commanded attitude, h_{RW} is the vector with level of each of the 4 reaction wheels of the Orbiter, \vec{k}_p , \vec{k}_i and \vec{k}_d are the proportional, integral and differential coefficients of the PID controller, and $\vec{L}(t)$ is the angular momentum of the system Orbiter-Lander with respect to the system's centre of mass in SC frame, which is calculated at each instant of time from the law of motion of the ejection mechanism, which is known.

3.2 Analysis of Orders of Magnitude

The results of the analysis of orders of magnitude during both the accelerated and the non-accelerated phases, considering the two extreme cases $\Delta v \sim 0.05$ m/s and $\Delta v \sim 0.5$ m/s, are provided in Table 2. The values also include orders of magnitude for rates and rotation angles.

Table 2: Order of magnitude of terms in differential equation along Y during separation. “*” denotes upper bound. The dominant torques during each phase are in bold.

	$\Delta v = 0.05$ m/s		$\Delta v = 0.5$ m/s	
	acc. phase	non-acc. phase	acc. phase	non-acc. phase
ω_y [rad/s]	$2 \cdot 10^{-4}$	$2 \cdot 10^{-4}$	$2 \cdot 10^{-3}$	$4 \cdot 10^{-3}$
$\Delta\theta_y$ [rad]	$9 \cdot 10^{-6}$	10^{-3}	$9 \cdot 10^{-4}$	10^{-3}
E_0 [Nm]	7	10^{-1}	7	$6 \cdot 10^{-1}$
E_{acc} [Nm]	7	0	7	0
E_p^{PID} [Nm]	$6 \cdot 10^{-4}$	$6 \cdot 10^{-2}$	$6 \cdot 10^{-2}$	10^{-1}
E_d^{PID} [Nm]	10^{-1}	10^{-1}	$4 \cdot 10^{-1}$	$4 \cdot 10^{-1}$
E_{exp} [Nm]	10^{-3}	$3 \cdot 10^{-3}$	10^{-1}	$6 \cdot 10^{-1}$
E_{gyr} [Nm]*	$5 \cdot 10^{-3}$	$5 \cdot 10^{-3}$	$5 \cdot 10^{-3}$	$5 \cdot 10^{-3}$
E_{env} [Nm]*	$2 \cdot 10^{-3}$	$2 \cdot 10^{-3}$	$2 \cdot 10^{-3}$	$2 \cdot 10^{-3}$

Table 3: Elements of the 1-D dynamic equations of separation subjected to order of magnitude analysis

Element	Definition	Description
E_0 [Nm]	$I_{comb,yy} \frac{a\omega_y}{dt}$	element with the highest order time derivative of the independent variable
E_{acc} [Nm]	$m_{comb}\ddot{s}d$	torque related to the acceleration of the Lander ejection mechanism
E_p^{PID} [Nm]	$k_{p,y}\theta_y$	torque related to the change in reaction wheel levels as a response to the request of the proportional component of the PID controller
E_d^{PID} [Nm]	$k_{d,y}\omega_y$	torque related to the change in reaction wheel levels as a response to the request of the derivative component of the PID controller
E_{exp} [Nm]	$\frac{dI_{comb,yy}}{dt} \omega_y$	torque related to the systems expansion, i.e. the fact that the inertia of the system increases as Orbiter and Lander separate from the centre of mass of the system
E_{gyr} [Nm]*	$(\vec{\omega} \times \vec{L})_y$	gyroscopic torque
E_{env} [Nm]*	N/A	environmental torque, with contributions from coma drag, nucleus gravity gradient and solar radiation pressure

The description of the elements on the table is as in Table 3.

The results of the analysis can be summarized as follows:

- For $\Delta v \sim 0.05$ m/s:
 - During the accelerated phase, only E_{acc} needs to be retained
 - During the non-accelerated phase, both E_d^{PID} and E_p^{PID} need to be retained
 - The depointing at separation is in the order of magnitude 0.05 deg (0.025 deg in the numerical solution)
- for $\Delta v \sim 0.5$ m/s:
 - During the accelerated phase, E_{acc} drives the movement and clearly dominates the equation; for very accurate predictions, E_d^{PID} might need to be considered
 - During the non-accelerated phase, E_d^{PID} drives the movement and the effect of E_{exp} is significant

- The depointing at separation is in the order of magnitude 0.1 deg (0.05 deg in the numerical solution)

Environmental and gyroscopic torques are negligible under any scenario.

3.3 Analysis of Sensitivity

As already mentioned, the driver of the rotational movement of the system Orbiter-Lander during separation is the acceleration of the Lander relative to the Orbiter induced by the separation mechanism. The associated torque is proportional to vector $\vec{r}_i \times \vec{e}$, where \vec{r}_i is the vector from the Orbiter to the Lander center of mass at the beginning of separation and \vec{e} a unitary vector in the direction of separation. An effective arm d, equal to the Y-component of vector $\vec{r}_i \times \vec{e}$, was defined. Because the depointing at separation is, in first approximation, proportional to the effective arm, the sensitivity of d to the following parameters was analyzed for both the maximum and minimum Orbiter masses expected at separation:

- **Position of the articulations (Solar arrays and High Gain Antenna):** The analysis of the range of possible articulation angles yielded an overall variability of the effective arm of $(d_{\max\text{mass}} - d_{\min\text{mass}}) / d_{\min\text{mass}} = 77.4\%$.
- **Propellant position in the tanks:** depending on the activities performed before the ejection, the propellant distribution could differ from the nominal case. The sensitivity to this distribution was studied taking into account the 6 cases in which the propellants were in contact with the tank walls in each of the coordinate directions. The worst case results are summarized in Table 4. As it can be seen, the variation

Table 4: Sensitivity of depointing to propellant mass position

Orbiter mass	Ejection speed	Nominal depointing around Y	Depointing around Y variation	Depointing around Z variation
Minimum	0.5 m/s	0.0501°	+/- 0.041°	+/-0.0042°
Maximum	0.5 m/s	0.0547°	+/- 0.054°	+/- 0.0055°
Minimum	0.05 m/s	0.0229°	+/- 0.0184°	+/- 0.0037°
Maximum	0.05 m/s	0.0252°	+/- 0.0244°	+/- 0.0049°

3.4 Effects of Separation on Reaction Wheels

In this section, we derive analytical expressions to estimate the Orbiter reaction wheel levels after attitude convergence following both the Lander fly-wheel spin-up and the Lander ejection processes.

3.4.1. Effect of Lander fly-wheel spin-up

The RW levels after attitude convergence could be estimated as:

$$\hat{h}_{RW,aft} = \hat{h}_{RW,bef} - H_{RW}^p \vec{h}_l$$

Equation 6

Where $\hat{h}_{RW,aft}$ and $\hat{h}_{RW,bef}$ are the 4-dimensional vectors containing the angular momentum of the wheels after and before the separation respectively, \vec{h}_l is the angular momentum of the

Lander fly-wheel in SC frame and H_{RW}^p is the 4x3 matrix that converts from angular momentum in SC frame to Orbiter wheel levels.

3.4.2. Effect of Lander Ejection

An expression to estimate the Orbiter reaction wheel levels after the Lander has been ejected from the Orbiter and the Orbiter attitude has converged back to its initial value was also derived. Since the main effect of the ejection process was concentrated on the Y-axis, an analysis of the RW angular momentum evolution around that axis sufficed. Equation 7 summarises this analysis, being $h_{y,2}$ and $h_{y,0}$ are the RW angular momentum around Y after convergence and before the ejection respectively, $m_{comb}\Delta vd$ is the driver of the ejection dynamical effects and $[I_{o,yy} - I_{comb,yy}(t_1)]\omega_{y,1}$ is the angular momentum to be absorbed due to the rate induced by the ejection process on the SC.

$$h_{y,2} = h_{y,0} + m_{comb} \Delta vd + [I_{o,yy} - I_{comb,yy}(t_1)]\omega_{y,1}$$

Equation 7

Equation 7 cannot be solved directly because it contains two unknowns, nominally $h_{y,2}$ and $\omega_{y,1}$. Therefore, further assumptions were introduced to be able to estimate $h_{y,2}$ from conservation of angular momentum. Two approximate solutions, each based on a different assumption were derived:

- Solution 1: RW levels remain constant within the ejection process. Assuming $h_{y,1} = h_{y,0}$, then $\omega_{y,1} = m_{comb}\Delta vd / I_{comb,yy}(t_1)$ and hence:

$$h_{y,2}^{min} = h_{y,0} + \frac{I_{o,yy}}{I_{comb,yy}(t_1)} m_{comb}\Delta vd$$

Equation 8

- Solution 2: Attitude remains constant within the ejection process. Assuming $\omega_{y,1} = 0$, Equation 7 leads to:

$$h_{y,2}^{max} = h_{y,0} + m_{comb}\Delta vd$$

Equation 9

3.5. Simulation of Separation

In order to verify the validity of the dynamic equations of separation presented in Section 4, as well as both the analytical and numerical results produced by these equations, the separation process was simulated with the SC emulator developed by the Flight Dynamics team at ESOC. This emulator, coded in Fortran, reproduces the AOCMS on-board software of the Rosetta spacecraft.

The emulator dynamic equations allowed to build a model of the ejection based on a thruster analogy which was close enough to the real equations of the movement. Consider the Orbiter and the Lander as independent systems. It is clear that the ejection takes place because the Orbiter performs a force on the Lander, and therefore, this force is received back by the Orbiter in the opposite direction causing the torque that leads to the rotation of the Orbiter around its Y axis. The value of such force is $F_{eje} = m_{lander}a_{lander}$. However, since there are additional constraints in the interface Orbiter-Lander (the rotation rate must be the same for both), some additional forces would appear in the direction perpendicular to the ejection speed. Both terms

should add up to yield a quantity equivalent to the E_{acc} term of the global system equation. Instead of analyzing the value of those additional forces and solving the isolated Orbiter problem, it can be shown that the main driver of the rotating movement can be matched by considering the torque of F_{eje} with respect to the Orbiter-Lander system CoM. Therefore, the problem was simulated as the firing of a thruster in the direction of the ejection during the acceleration time still considering the Lander as part of the system.

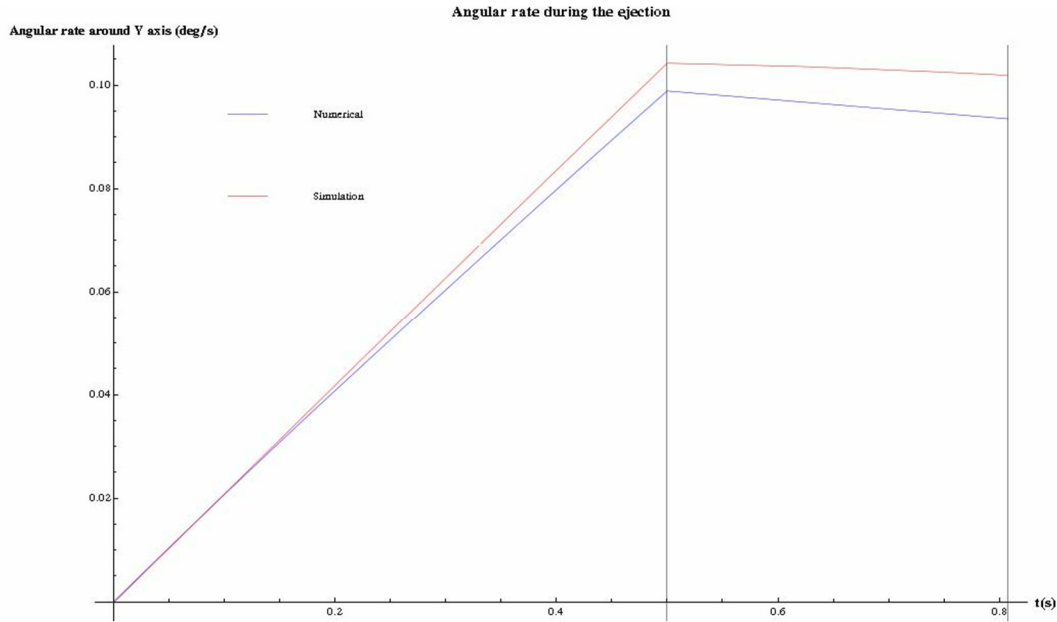


Figure 10: Angular rate around SC y-axis during ejection. Blue: numerical. Red: simulation.

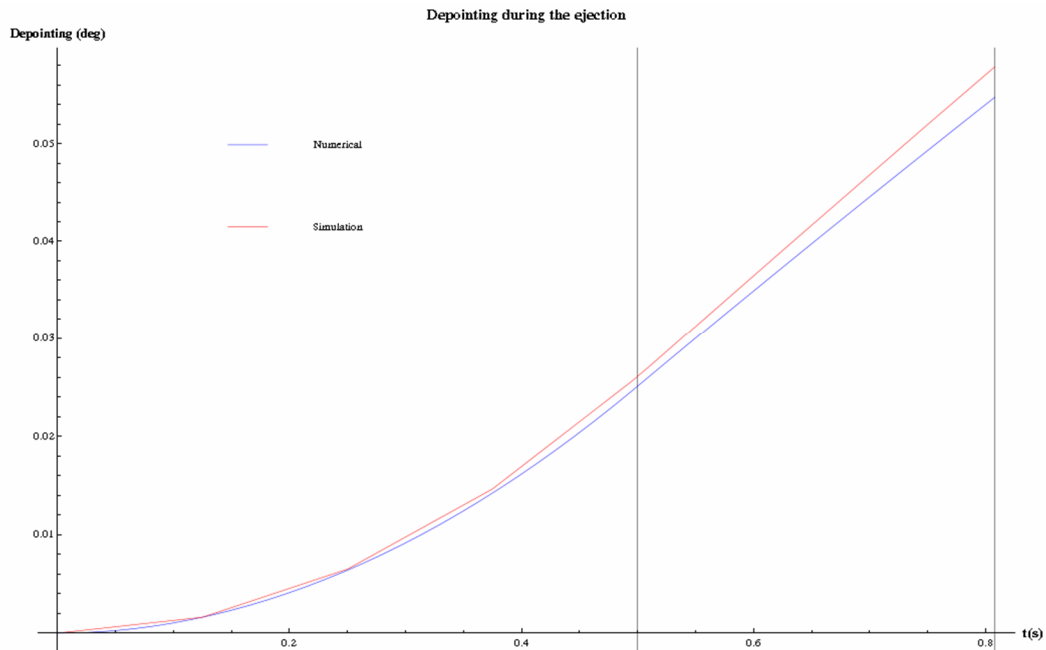


Figure 11: SC depointing during ejection. Blue: numerical. Red: simulation.

Figure 10, Figure 11, Figure 12 and Figure 13 show the results obtained for the maximum ejection Δv (0.5 m/s) compared against a numerical integration of the equations of motion. Figure 10 shows the evolution of the y-rate during the ejection process, increasing during the accelerated phase and slowly controlled afterwards. Figure 11 shows the evolution of the y-depointing during the ejection process reaching a maximum value of ~ 0.05 degrees. Figure 12 shows the convergence of the y-depointing after the ejection. It can be seen that the maximum depointing reached is around 0.5 degrees and that the convergence time is in the order of a minute.

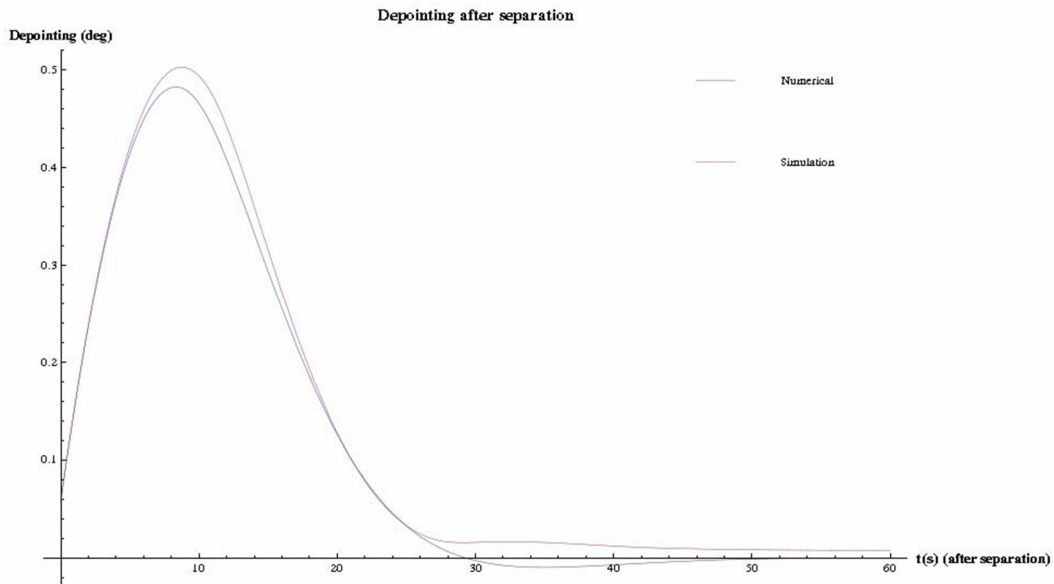


Figure 12: SC depointing after ejection. Blue: numerical. Red: simulation.

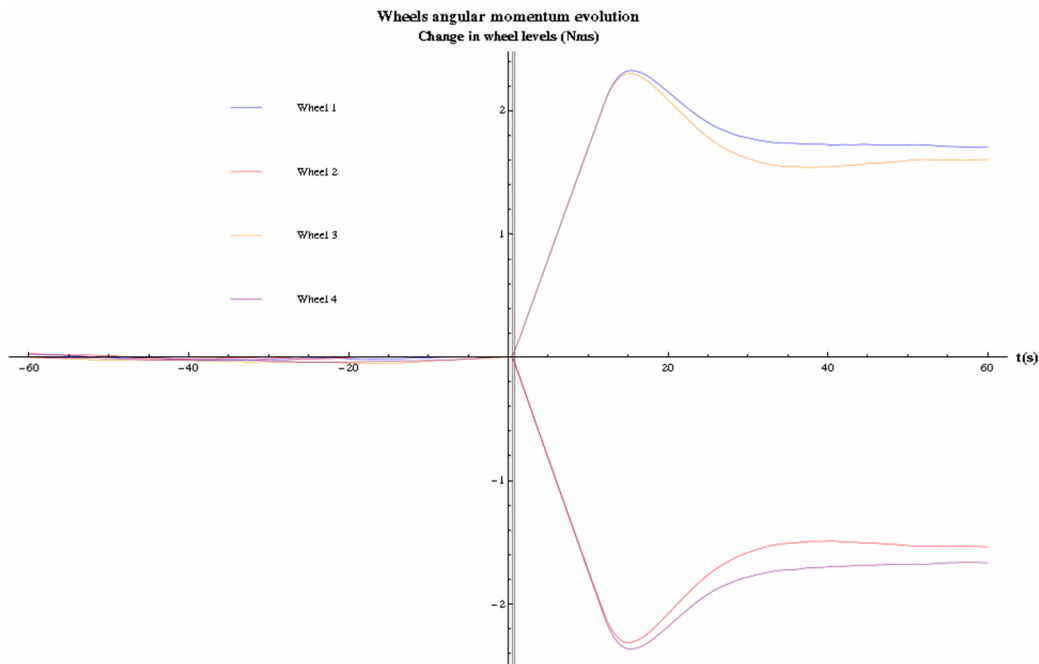


Figure 13: Reaction Wheel delta angular momentum after ejection. Blue: RW1; Red: RW2; Orange: RW3; Purple: RW4.

Finally, Figure 13 shows the simulated evolution of the Reaction Wheel levels after the ejection, with the wheels starting from 0 Nms. A 2 Nms variation in the angular momentum of each wheel was expected.

3.6. Summary of analyses

The analysis concluded that the typical depointing of the system Orbiter-Lander when the Lander reached the end of the spindle was in the order of 0.05 deg. Since the directional uncertainty of the ejection direction was 0.3 deg at 1 σ , much larger than the expected rotation induced by the separation process, the proposed strategy was to neglect the angular offset introduced by the separation process and command a SC attitude quaternion such that the Lander attitude before separation is equal to the target Lander attitude right after separation, the latter being defined by the optimization of the Lander descent trajectory. Moreover, it was shown that the position of the SC High Gain Antenna (HGA) introduced a variability in the depointing at separation up to 80%, whereas the variability associated with the propellant position in the tanks was up to 100%, leaving little room for an accurate attitude pre-compensation strategy. Finally, the Orbiter attitude off pointing during the tranquillization period following Lander separation was shown to be below 1 degree, which was important to ensure that no FDIR mechanisms would be triggered following the ejection and therefore impacting the landing support activities of Rosetta.

4. Rosetta timeline of activities and attitude profile design

4.1. Rosetta timeline of activities for Philae's landing operations

A detailed description of the Lander Delivery timeline from the Orbit Design point of view is already covered in detail in an accompanying paper [6], therefore only the main points will be highlighted here. In the scope of this paper the interval between \sim -12 hours and \sim +12 hours from separation time is considered. This Lander Delivery phase was characterised by a very tight operational schedule since, in addition to the Lander ejection itself, it had to accommodate three OCMs, three RW Off-Loadings, three large attitude slews and a number of other activities.

The three manoeuvres are:

- Predelivery OCM, to inject the SC from the initial parking orbit in the Comet's terminator, to a trajectory arc passing over the target Lander release point. This manoeuvre had a magnitude of about 0.836 m/s and a duration of around 6'. Note that, the start time of this OCM was a degree of freedom available to the Manoeuvre Optimisation Team (MAN) and was only constrained to be in the interval [-3,-2] hours from separation time.
- Postdelivery OCM, executed 40' after Lander ejection, with the SC in the same attitude. The objective of this manoeuvre was that of having the Orbiter 'above' the Lander w.r.t. the Comet in order to take images of its descent for trajectory reconstruction. The magnitude was 0.6 m/s and the duration was about 5'.
- Relay-Phase Manoeuvre 1 (RP-1), to insert the Orbiter in an orbit designed to maximise communication opportunities with the Lander.

In terms of attitude pointing history, one can identify four different phases, connected by three large slews.

- From -12 hour up to the Predelivery OCM the SC was commanded to an attitude corresponding to the latest prediction of the manoeuvre direction itself, as explained in

Section 2.4. Note that the Predelivery OCM was expected to be recalculated during this interval according to the latest OD and therefore the attitude would have been slightly adjusted accordingly.

- After the Predelivery OCM the SC performed a 45' slew, in order to reach the separation attitude. The latter was defined such the ejection direction (close to the SC $-x$ axis) be aligned with the ejection ΔV computed by MAN; similarly the SC $+z$ axis was constrained to be aligned with the Postdelivery OCM direction. In this way, this OCM could be performed within a short time after Lander ejection without an attitude slew.
- After OCM completion the SC performed a wide angle slew (~ 160 deg) to point the $+z$ axis to the predicted Lander direction. As will be shown in the next Section, the design of this slew posed a considerable challenge, since it was highly desirable to point the Lander as soon as possible, provided orbit geometry and SC constraints allowed this. The minimum time foreseen for this slew was 30'.
- In the Lander-Imaging pointing the SC performs raster imaging around the nominal Lander direction. The raster cycle was 1 hour with pictures taken at 4 positions offset by ± 4.5 degrees around the SC x and y axes. The Imaging phase terminated 2 hours 20' after expected touchdown time.
- After the end of the imaging the SC performed a 1hr slew to the RP-1 attitude.

Each OCM is also preceded by a WOL, this being routine operational practice for the Rosetta mission, although in the present case the first two WOLs had a key role for angular momentum management:

- The Predelivery WOL was also the first being executed after the spin-up of the Lander flywheel (corresponding to an angular momentum of 5.17Nms along $+z$) and therefore was targeted at compensating this contribution until separation.
- The Postdelivery WOL, which adsorbed the angular momentum contribution of the ejection ΔV and of the 'removal' of the flywheel contribution. Without this WOL, the relatively fast slew from separation attitude to Lander pointing would have hardly been possible due to constraints on maximum RW angular momentum.

In terms of SC modes and subsystems operation, the activities related to OCMs, WOLs and slews will not be detailed here as these are part of routine operation of Rosetta. The focus will be on special actions and commands introduced in the scope of Philae ejection:

- From $\sim 9'$ before separation, when the SC is in fixed attitude, the drive electronics for the HGA and Solar Arrays (SA) were switched from auto-tracking mode to off. This was in order to prevent that small movements of these appendages could perturb the attitude around the critical moments of ejection.
- 30s before separation the AOCS was switched from Fine-Pointing Attitude mode (FPAP) to Wheel-Controlled Damping mode (WDP). While in the former the AOCS control parameters are tuned for optimum accuracy (and as such this mode is normally used for Science pointings etc.), in the latter the control tuning was aimed at torque disturbances rejection. In this sense, the transition to this mode right before separation was aimed at a quick compensation of attitude disturbances due to ejection. Note that the choice to delay the switch to WDP at 30" before separation was due to the intrinsic lower accuracy of WDP, which could have led to an increase of the depointing over time.

Several GO/NOGOs points were scheduled in the hours leading to separation, requiring assessment of certain preconditions by the main actors (Flight Control Team, Flight Dynamics, Lander Team etc.). In the scope of this analysis, it is relevant to mention the final GO/NOGO

step based on assessment of performance of the Predelivery OCM. If the latter did not meet a precise set of requirements, the telecommands (TCs) to initiate the separation process would not have been sent and the Rosetta SC was foreseen to fly the rest of the timeline unaltered but with the Lander still attached. On the contrary, if the OCM performance was judged as satisfactorily, the TCs to initiate the separation sequence would be sent such that they would reach the SC as soon as its HGA was again in Earth tracking. As reported in Table 5, this could have been as late as just 30' before separation and in this sense there was not enough time to wait for the TC reception confirmation signal to reach the Earth (the one-way light time between Comet and Earth being about 25').

Table 5: Lander delivery timeline. Legend: Orange-Lander events. Blue-WOLs. Green-OCMs. Purple-SC AOCs events. Pink-GO/NOGOs.

Rel. time earliest / (latest)	Event	Notes	SC Attitude	SC Orbit arc
-12:20:00	SC reaches Pre-Delivery OCM	OCM attitude as predicted in previous OD.	Pre-delivery OCM attitude	Pre-delivery parking orbit
-12:11:00	Lander flywheel spin-up			
-04:35:00		Start of Lander Delivery VSTP		
-04:30:00	Start of Pre-Delivery WOL	Contribution of flywheel angular momentum is compensated.		
-04:05:00/ (-03:05:00)	Start of slew to Pre-Delivery OCM attitude	A small attitude adjustment as a result of OD since the SC was already commanded in the (predicted) OCM attitude in the previous VSTP		
-03:05:00/ (-02:05:00)	SC in OCM attitude			
-03:00:00/ (-02:00:00)	Pre-Delivery OCM starts			
~-02:30:00/ (-01:30:00)	OD assessment of OCM performance	Criterion for Final GO/NOGO		
-02:15:00/ (-01:15:00)	Start of slew to Separation attitude			
-01:30:00/ (-00:30:00)	SC reaches separation attitude			
-00:25:00	Latest time at which GO command shall be received by SC	Command to abort Separation sequence is executed instead		
-00:20:00	On-board separation sequence starts		Separation attitude	
-00:09:30	SADE to SBY and OFF			

~-00:09:00	Cruise safety latch opened	Lander held by release spindle motors only		
-00:07:30	APME to SBY and OFF			
-00:00:30	Switch to WDP			
+00:00:00	SSP separation			
+00:12:00	Switch to FPAP	End of tranquilisation phase		
+00:15:00	Start of Post-Delivery WOL	Compensates contribution of separation ΔV and flywheel		
+00:40:00	Start of Post-Delivery OCM			Lander imaging arc
+01:15:00	Start of Slew to Lander Imaging		Slew	
+01:45:00/ (+02:15:00)	End of slew to Lander imaging	First image of the Lander taken around this time	Lander pointing with Rasters	
+07:00:00	Nominal touchdown			
+09:20:00	End of Lander imaging phase	End of Lander Delivery VSTP	Nadir pointing	
+09:25:00	Start of WOL			
+09:50:00	Start of slew to RP-1 OCM attitude		Slew	
+10:50:00	SC in RP-1 OCM attitude.		RP-1 OCM attitude	
+10:55:00	Start of RP-1 OCM			Relay arc 1

4.2. Design of Lander Imaging Attitude

The design of the attitude profile for the Lander imaging phase after separation posed a considerable challenge due to the conflicting set of constraints, namely:

1. The SC z-axis shall point towards the (predicted) Lander position for taking pictures.
2. The angle of the Sun direction and the SC x-z-plane shall be below 30 deg, in order to have sufficient incident radiation on the SA for power generation. Note that, since the SA rotation axis is along +/-Y, this angle corresponds to the Sun Aspect Angle (SAA) on the SA.
3. The angle of the Sun direction on the SC x-z-plane shall be between 0 deg and 192 deg (angle counted from +z towards +x). This is due to illumination constraints on radiator surfaces.

Constraint 1 effectively reduced the number of degrees of freedom to one, i.e. the rotation angle φ around the SC z-axis. Constraints 2 and 3 on the other hand severely restricted the domain of φ , depending on the Sun-SC-Lander angle.

In addition the following requirements were also applicable:

- a. The slew from separation to imaging attitude shall be performed as quickly as feasible, compatibly with dynamical limitations due to RW and other constraints (e.g. maximum attitude rate and acceleration, maximum RW angular momentum).
- b. The attitude profile definition shall be robust against expected uncertainties on the trajectory design.
- c. The attitude profile shall be generated by the CMD team within the tight schedule of Lander delivery operations.

Requirement a. indirectly translates into a requirement on φ , since, as a first approximation, the smaller the angular distance between the initial and final attitude quaternions, the faster will be the slew to connect them. From the point of view of Lander descent trajectory reconstruction, it was highly desirable to start taking imaging of the Lander as soon as possible, and therefore it was aimed at performing the slew to imaging attitude in 30'. To put this into perspective, one has to consider that in routine operational phases, attitude slews are sized for a fixed value of 60', because with such duration it is possible to accommodate for any geometric configuration of initial and final attitude, within the given set of attitude and other dynamic constraints. However, in the scope of the Lander imaging phase, such a long slew would have most likely led to missing the images when the latter was closer to Rosetta.

A simple way to satisfy Constraints 1 to 3 is that of flying an attitude which is geometrically defined as follows:

- The z-axis points the Lander.
- The y-axis is aligned with the normal to the vector product of the Lander and Sun direction.

Note that with this geometrical formulation the SAA on the SA is minimum and therefore the solar power generated is at its theoretical maximum; for this reason, this type of attitude profile will be referred to as *Power-Optimised* attitude and the corresponding time law for the rotation angle will be called $\varphi_{PwrOpt}(t)$. Again the issue is that, due to the geometry of the Lander delivery trajectory, slewing from Separation to the Power Optimised attitude might take too long. In this sense, it might be more advantageous to slew to an attitude with an offset $\Delta\varphi$ with respect to the Power Optimised profile in order to contain the slew duration within 30'.

In order to define the slew and imaging attitude profiles, a simple and robust logic was defined and implemented into an algorithm. The main steps of this procedure are shown in Figure 14. The full mathematical formulation of the problem and its detailed algorithmic implementation have been omitted here for sake of conciseness.

The objective of the process is that of defining the slew duration Δt_{slew} and the time law $\varphi(t)$ for the rotation angle around z-axis over the interval $[t_a, t_b]$. The procedural steps are as follows:

1. The initial Δt_{slew} is assumed to be the desired minimum duration of 30'.
2. The slew from Lander Ejection attitude to the Power-Optimised, Lander-Pointing attitude is calculated for duration Δt_{slew} is calculated.
3. If the slew calculated at the previous step is feasible from the point of view of dynamical and RW constraints, the algorithm terminates. The output attitude profile is simply $\varphi_{PwrOpt}(t)$ in the interval $[t_{endslew}, t_b]$.

4. Otherwise, the algorithm searches for a fixed offset angle $\Delta\varphi$ from $\varphi_{PwrOpt}(t)$, for which constraints are satisfied for the first two rasters (of duration $\Delta t_{rast} = 60'$) after the end of the slew. In order to do this, the algorithm scans the interval $[t_{endslew}, t_{endslew} + 2\Delta t_{rast}]$ and saves the values of $\Delta\varphi$ for which no attitude constraint is violated. Let one define this set as $\Delta\Phi_{feas1}$.
5. The slew feasibility is checked in a similar way to step 0 for the attitude profile corresponding to each $\Delta\varphi \in \Delta\Phi_{feas1}$. Those corresponding to a feasible slew belong to the set $\Delta\Phi_{feas2} \subset \Delta\Phi_{feas1}$.
6. If none of the $\Delta\varphi$ can be reached with a slew of the desired duration Δt_{slew} , the latter is increased by half the duration of a raster, i.e. $30'$, and the algorithm goes back to step 0.
7. Otherwise, the optimum offset angle $\Delta\varphi_{opt}$ is chosen as the minimum $\Delta\varphi \in \Delta\Phi_{feas2}$, i.e. the closest to the Power-Optimised attitude.
8. The attitude profile is thus defined as follows:
 - In interval $[t_{endslew} = t_a + \Delta t_{slew}, t_{endslew} + 2\Delta t_{rast}]$ the attitude is offset by an angle $\Delta\varphi$ around z-axis with respect to the Power-Optimised profile $\varphi_{PwrOpt}(t)$.
 - In interval $[t_{endslew} + 2\Delta t_{rast}, t_{endslew} + 2.5\Delta t_{rast}]$ the SC performs a rotation around z-axis to reach the Power-Optimised profile $\varphi_{PwrOpt}(t)$.
 - In interval $[t_{endslew} + 2.5\Delta t_{rast}, t_b]$ the SC flies the Power-Optimised profile $\varphi_{PwrOpt}(t)$.

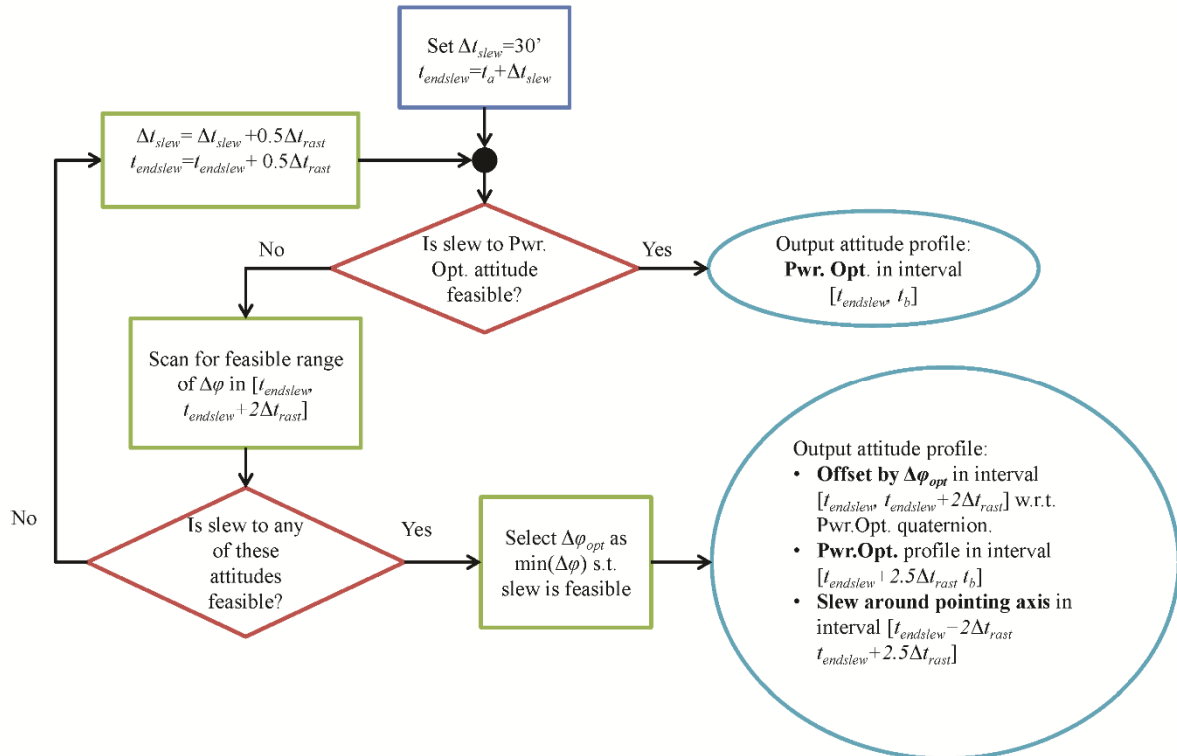


Figure 14: Flowchart of Algorithm for Lander Imaging Attitude design.

The proposed algorithm allowed to automatically tailor the attitude profile definition to the specific geometry of the Lander Delivery trajectory, adapting the Lander Imaging attitude profile as required to minimise the duration of the post-ejection slew. The algorithm was thoroughly and

successfully tested for robustness on a set of trajectories generated by the MAN team as a result of Montecarlo analysis. In its actual use during Lander Delivery operations, it allowed to slew to the Lander Imaging attitude at the earliest possible time, i.e. 1hr15' after ejection and thus take the first images of the Lander when the latter was still very close to Rosetta.

5. Results from Philae's landing operations

The timeline of activities presented in Section 4.1 was followed without encountering any contingency over the course of the evening of the 11th of November and the night and early morning of the 12th. The preparation of the FD commands for the Lander delivery period, spanning from 04:00 to 17:55 UTC of the 12th, started at the data cut-off set for 14:00 UTC of the previous day. The FD cycle consisted in the processing of 10 rasters of 4 images from the previous 12 hours to generate 2452 observations of 721 landmarks, an orbit determination process spanning about a month of radiometric and optical data, the final tuning of the ΔV optimization for two manoeuvres and the Lander separation, and the generation of all commands for the complex timeline of activities of Table 5. This sequence was completed around 22:00 UTC, two hours in advance of the deadline for the availability of the FD products set at 00:00 UTC of the 12th. This allowed giving the first Go for Lander separation. During the evening and then the night, two additional Gos were given on the basis of the status of the Rosetta SC and of the Philae Lander. Finally, the last Go/Nogo for separation was foreseen at 06:30 UTC, only ~20 minutes after the pre-delivery OCM data were received on-ground. This was based on a quick assessment of the spacecraft TM during the manoeuvre and of the Doppler residuals indicating the ΔV error. The former are presented in Figure 15, showing that the STR continued to track a sufficient number of stars and that the control system ensured an attitude off-pointing of less than 70 mdeg (Go/Nogo criteria were >2 stars and <0.5 deg). The latter are instead detailed in a separate paper ([6]), which analyses Rosetta and Philae navigation activities during landing.

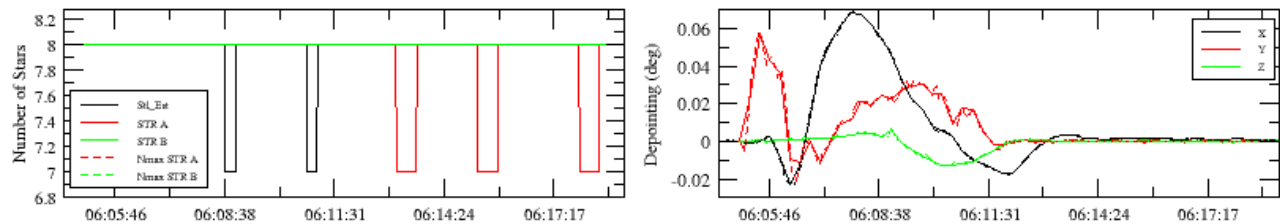


Figure 15: Number of tracked stars and SC off-pointing during the pre-delivery OCM.

It is however worth noting here, that the final error on the pre-delivery OCM was limited to 1.2 mm/s out of nominal 835.8 mm/s, i.e. less than 0.15%. This extremely good performance, sensibly better than the required 0.5%, is almost entirely due to the accelerometer bias calibration strategy described in Section 2.4. During the night, calibrations were performed continuously, with the purpose of assessing the thermal stabilization of the IMPs and their effect on the OCM performance. The last slot for the commanding of a bias update was foreseen only 2 hours before the OCM, and it was indeed decided to exploit it, since the values had been continuing to vary. Figure 16 shows the bias estimates over the course of 11th and 12th of November, expressed in percentage difference with respect to the last commanded value, received on-board only around 04:30 UTC for a manoeuvre start at 05:35 UTC. The graph confirms that, had the calibration been done in a different attitude (e.g. data points on the right, referred to the imaging phase), the error on the OCM may have exceeded 0.5%, resulting in Nogo for separation. Moreover, it is

clear how even the latest calibration data contributed to further improving the accuracy of the OCM, which was key to the achievement of a final landing point error of merely 118 meters on the surface of the comet, whereas the landing ellipse size from the Lander navigation analyses was in the order of the 500 m radius.

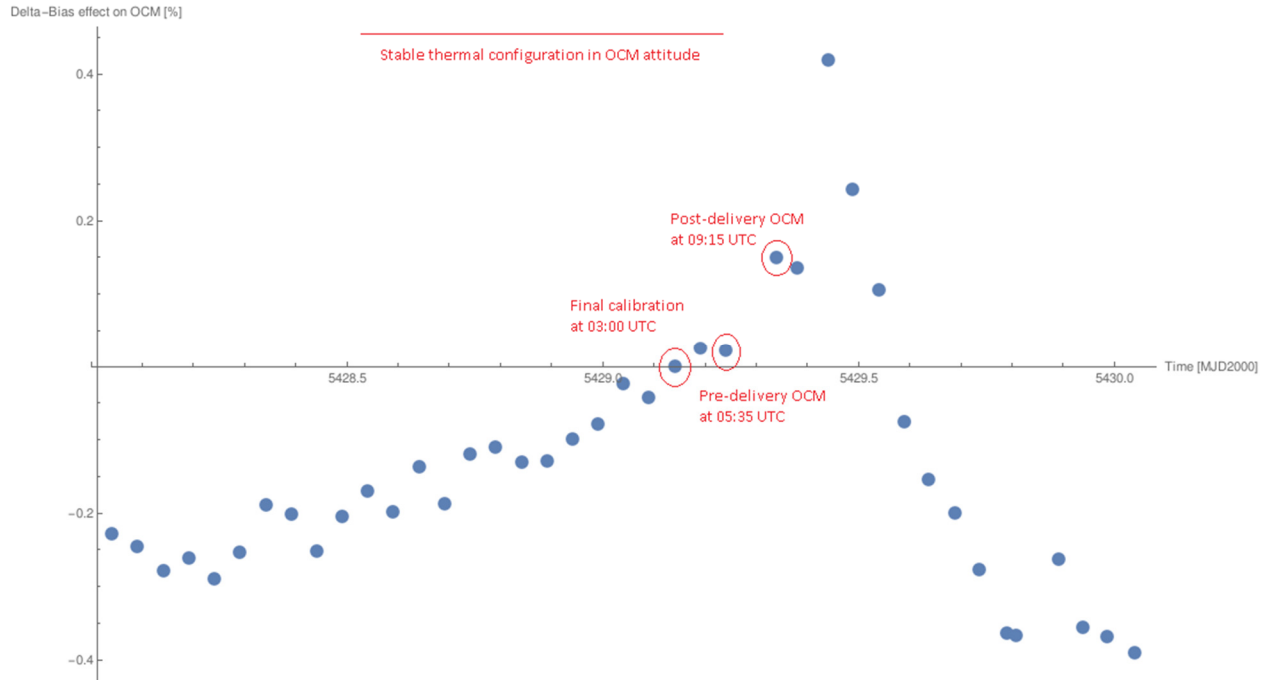


Figure 16: Accelerometer bias estimates over the 11th and 12th of November, in percentage difference with respect to the bias commanded on-board with the final calibration ~ 2.5 hours before the pre-delivery OCM i.e. $(b_{zsc}(j) - b_{zsc}(t=03:00)) \cdot t_{OCM} / \Delta V_{OCM} \cdot 100$

The live FD activities were concluded with the final Go/Nogo for separation based on the OCM performance. FD work during the separation and descent phases was focused on the assessment of the separation performance and on the reconstruction of Philae's landing trajectory from separation to (first) touch-down. Although with no operational impact, these were extremely interesting - and for some aspects particularly challenging - activities, and a detailed overview is given in [6]. Some results on the separation dynamics are instead reported here in Figure 17, Figure 18 and Figure 19, which show respectively the SC rate from 8 Hz TM around the Y axis during the first 10 seconds of ejection, the wheels speed absorbing the separation angular momentum and being successively off-loaded, and the SC rates and off-pointing on the 3 axes during separation and WOL. These data confirm the validity of the separation dynamics analyses described in details in Section 3, although the values presented there were referred to the worst case of 50 cm/s separation ΔV , whereas the result of the final optimization led to the tuning of the ejection mechanism for only 17.4 cm/s. It is however clear that the most important separation decision - of not pre-compensating the SC attitude - was indeed correct, as the maximum rate on the Y axis only reached ~ 40 mdeg/s, resulting in an attitude error for the Lander of less than 20 mdeg (i.e. 0.5 s into the separation) and a maximum SC off-pointing of around 0.1 deg.

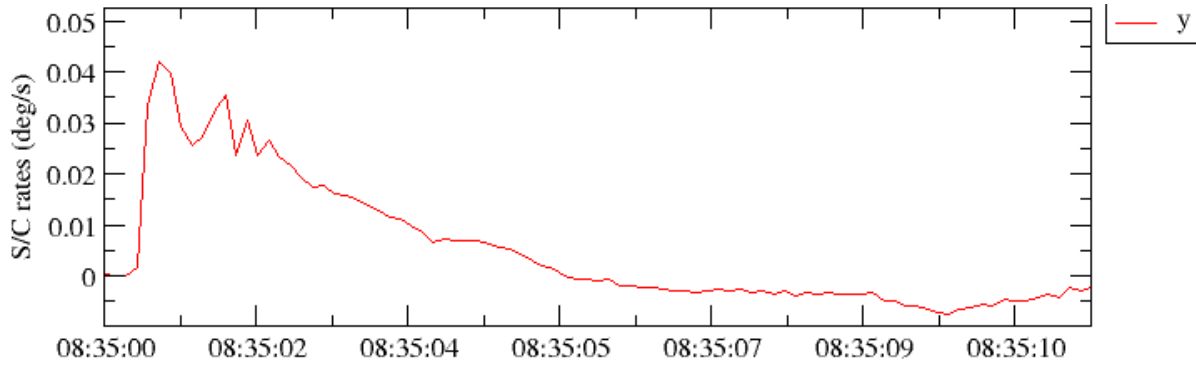


Figure 17: SC rate on the Y axis from 8Hz TM during the Lander ejection.

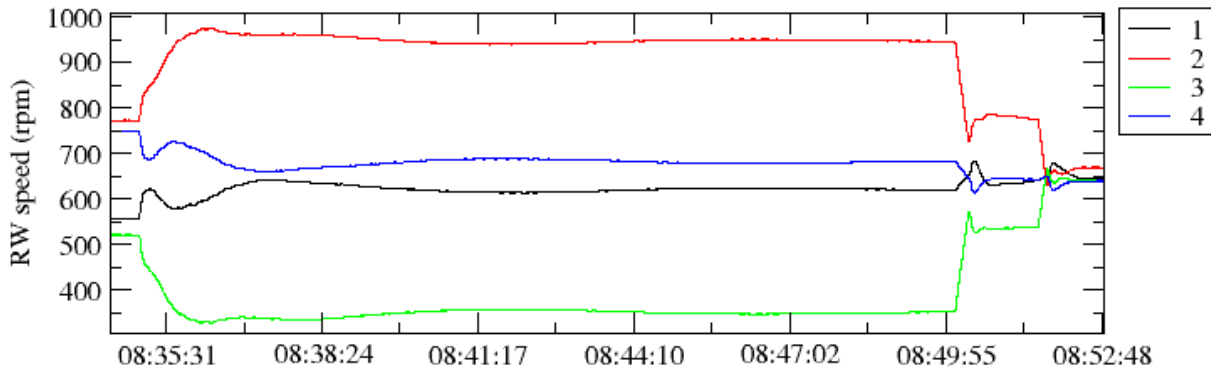


Figure 18: SC RW speeds from Lander separation to the successive wheel off-loading.

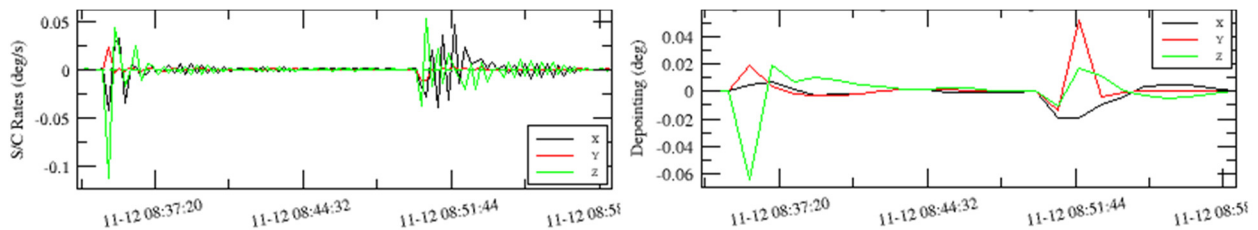


Figure 19: SC rates and offpointing from Lander separation to successive wheel off-loading.

5. Conclusions

The paper presented a series of telemetry reductions, dynamic analyses and design activities which were carried out by ESOC's Flight Dynamics team in preparation and for real time support of Philae's landing. The focus was on the AOCMS monitoring and commanding side rather than on the navigation point of view, presented in a complementary paper ([6]).

Detailed SC health evaluations in the weeks leading to the landing were fundamental to assess the suitability of the platform to perform the required complex set of activities during few hours around Lander separation. In particular, the robustness of sun sensors and star trackers to the comet's dust environment was verified, and specific measures were taken to minimize the stress on wheel C, showing initial signs of degradation. Moreover, an analysis of the accelerometers bias from SC reactivation allowed to select IMP-A as the most accurate for manoeuvre cut-off, due to the lower effect in the thrust direction of bias variations with respect to IMPs B and C. The same analysis also led to the decision of including in the landing timeline a calibration slot

of 12 hours in the pre-delivery manoeuvre attitude with all instruments in stand-by, in order to reduce as much as possible the residual bias error.

In parallel, very detailed analytical and numerical analyses of the Lander ejection process allowed to accurately simulate the behaviour of the system during separation, leading to the decision of not pre-compensating the SC attitude before Lander ejection. This and several other analysis activities informed the design of a very complex timeline of commands and events and of a similarly complicated attitude profile for the Rosetta spacecraft. Results are presented in the paper from the SC telemetry during the landing operations, confirming that all the described monitoring, analysis and design activities were instrumental for successfully completing the very complicated series of tasks for both spacecraft and ground control team that led to the landing of Philae. It was in fact the diverse activities described in this paper, together with a robust attitude and trajectory design, accurate landmark optical navigation and flawless performance of the spacecraft platform, that allowed to bring the Lander at a touch-down point 118 meters away from the target landing coordinates on the smaller lobe of comet 67P/Churyumov-Gerasimenko, after a purely ballistic descent in an active comet environment.

References

- [1] Budnik F., Companys V., Lauer M., Fertig J., Morley T., Godard B., Munoz P., Casas C., and Janarthanan V., “Rosetta: Comet Approach and Proximity Navigation”, Proceedings of 25th International Symposium on Space Flight Dynamics (ISSFD), Munich, Germany, October 2015.
- [2] Castellini F., Antal-Wokes D., Pardo de Santayana R., and Vantournhout K., “Far Approach Optical Navigation and Comet Photometry for the Rosetta Mission”, Proceedings of the 25th International Symposium on Space Flight Dynamics (ISSFD), Munich, Germany, October 2015.
- [3] Pardo de Santayana R., and Lauer M., “Optical Measurements For Rosetta Navigation Near The Comet”, Proceedings of the 25th International Symposium on Space Flight Dynamics (ISSFD), Munich, Germany, October 2015.
- [4] Morley T., Budnik F., Godard B., Munoz P., and Janarthanan V., “Rosetta Navigation from Reactivation until Arrival at Comet 67P/Churyumov-Gerasimenko”, Proceedings of 25th International Symposium on Space Flight Dynamics (ISSFD), Munich, Germany, October 2015.
- [5] Godard B., Budnik F., Munoz P., Morley T., and Janarthanan V., “Orbit Determination of Rosetta Around Comet 67P/Churyumov-Gerasimenko”, Proceedings of 25th International Symposium on Space Flight Dynamics (ISSFD), Munich, Germany, October 2015.
- [6] Munoz P., Budnik F., Companys V., Godard B., Casas C., Morley T., and Janarthanan V., “Rosetta Navigation During Lander Delivery Phase and Reconstruction of Philae Descent Trajectory and Rebound”, Proceedings of 25th International Symposium on Space Flight Dynamics (ISSFD), Munich, Germany, October 2015.
- [7] Pardo de Santayana R., Lauer M., Muñoz P., and Castellini F., “Surface Characterization And Optical Navigation At The Rosetta Flyby Of Asteroid Lutetia”, Proceedings of the 24th International Symposium on Space Flight Dynamics (ISSFD), Laurel, MD, May 2014.
- [8] Antal-Wokes D.S., and Castellini F., “Rosetta: Imaging Tools, Practical Challenges and Evolution of Optical Navigation around a Comet”, Astrodynamics Specialists Conference 2015, Vail, CO, August 2015.